metals

MDPI

Article

Microstructural Evolution and Mechanical Behavior of TA15 Titanium Alloy Fabricated by Selective Laser Melting: Influence of Solution Treatment and Aging

Qing Wang [1], Binquan Jin [1], Lizhong Zhao [1], Xiaolian Liu [1], Anjian Pan [1], Xuefeng Ding [2,*], Wei Gao [2], Yufeng Song [2] and Xuefeng Zhang [1,*]

[1] Institute of Advanced Magnetic Materials, College of Materials and Environmental Engineering, Hangzhou Dianzi University, Hangzhou 310018, China; wq15505086285@163.com (Q.W.); jinbinquan2000@163.com (B.J.); lzzhao@hdu.edu.cn (L.Z.); liuxiaolian@hdu.edu.cn (X.L.); ajpan@hdu.edu.cn (A.P.)

[2] College of Mechanical and Electrical Engineering, Hunan University of Science and Technology, Xiangtan 411201, China; 18356698440@163.com (W.G.)

* Correspondence: dingxf0910@163.com (X.D.); zhang@hdu.edu.cn (X.Z.)

Abstract: In this study, TA15 titanium alloys were successfully prepared using selective laser melting (SLM). The results show that the microstructure of each TA15 specimen is composed of a large number of acicular α′ martensite crystals accompanied by a lot of dislocations and twin structures in the martensite due to non-equilibrium heating and cooling via SLM. After solution treatment and aging treatment, the martensite structure is successfully transformed into a typical duplex structure and an equiaxial structure. When there is an increase in the solution temperature, the size of the equiaxed primary α phase and the elongation of the specimen gradually increases, while the thickness of the layered secondary α phase and the tensile strength of the specimen decreases accordingly. After solution treatment at 1000 °C, the specimens show the best comprehensive mechanical properties, i.e., a high-temperature tensile strength of 715 MPa and a corresponding elongation of 24.5%. Subsequently, an appropriate solution–aging treatment is proposed to improve the high-temperature mechanical properties of SLMed TA15 titanium alloys in aerospace.

Keywords: SLM; solution and aging treatment; mechanical properties; TA15 titanium alloy

check for updates

Citation: Wang, Q.; Jin, B.; Zhao, L.; Liu, X.; Pan, A.; Ding, X.; Gao, W.; Song, Y.; Zhang, X. Microstructural Evolution and Mechanical Behavior of TA15 Titanium Alloy Fabricated by Selective Laser Melting: Influence of Solution Treatment and Aging. *Metals* **2023**, *13*, 1514. https://doi.org/10.3390/met13091514

Academic Editors: Thomas Niendorf and Andrea Di Schino

Received: 15 June 2023
Revised: 14 August 2023
Accepted: 18 August 2023
Published: 24 August 2023

Copyright: © 2023 by the authors. Licensee MDPI, Basel, Switzerland. This article is an open access article distributed under the terms and conditions of the Creative Commons Attribution (CC BY) license (https://creativecommons.org/licenses/by/4.0/).

1. Introduction

TA15 (Ti-6Al-2Zr-1Mo-1V) is a near-α-type titanium alloy which has both the good thermal strength and weldability of α-type titanium alloy and the process plasticity of α-β-type titanium alloy. It has been widely used in aerospace, bearing parts, and engine structures because of its high-temperature performance, fracture toughness, and corrosion resistance [1–3]. However, owing to the high activity, deformation resistance, and low thermal conductivity of titanium alloys, the traditional melt casting and welding methods have some shortcomings, such as high equipment requirements, complex processes, low material utilization rates, and long production cycles, etc., making it difficult to prepare TA15 titanium alloy structural parts with complex shapes and structures [4–7]. Therefore, it is necessary to explore a new process to prepare titanium alloy parts with complex structures [8].

As a new type of metal additive manufacturing technology (AM), SLM uses a high-energy laser beam to scan pre-laid metal powder according to the predetermined scanning path, and the powder is then completely melted, cooled, and solidified, which can effectively reduce the cost, shorten the cycle, and improve the utilization rate of materials. SLM technology can manufacture metal parts with complex shapes and structures [9,10]. In recent years, SLM has proved to be a promising manufacturing method for TA15 titanium

alloys. Xu et al. [11] successfully prepared Ti-6Al-2Zr-1Mo-1V (TA15) titanium alloys with ultra-fine crystals and many nanoscale twins using SLM, and the tensile properties of the SLM specimens at room temperature and a high temperature (500 °C) were significantly higher than those produced using conventional technology. Cai [12] prepared high-density and high-strength TA15 titanium alloys by optimizing the process parameters of SLM (laser power, scanning speed, and scanning distance), and their performance was significantly higher than that of as-cast TA15 titanium alloys. Jiang [13] prepared nearly full-density TA15 titanium alloys using SLM, and the tensile strength at room temperature reached 1296 MPa, 35% higher than that of as-cast materials. These studies have demonstrated the feasibility of the SLM-based preparation of TA15 titanium alloys. Due to the technical characteristics of SLM, i.e., the non-equilibrium heating and cooling of thermal cycles at different peak temperatures, many α´ needle martensite crystals are found in the TA15 titanium alloy parts prepared via SLM. The martensite is unstable and prone to decomposition at a high temperature, which restricts its further application in aerospace.

The preparation process determines the microstructure of titanium alloys. Heat treatment can effectively improve the microstructure of titanium alloys and regulate their mechanical properties. Li et al. [14] annealed the forged TA15 titanium alloy at 810 °C to 995 °C and found that the content of the primary α phase decreased while the content of the secondary α phase increased, resulting in a decrease in the plasticity of the specimen but an increase in the strength. Sun et al. [15] performed a two-phase field heat treatment on a conventionally forged TA15 titanium alloy. Obtained via the equiaxed α phase, the lamellar α phase and transformed β matrix composed of a tri-modal microstructure have excellent comprehensive mechanical properties. Wu et al. [16] performed single-phase field heat treatment and single-phase + two-phase field heat treatments on forged TA15, and a lamellar microstructure, basket weave microstructure, two-phase composite microstructure, and tri-modal microstructure were obtained in forging (α + β phase zone) combined with high-temperature aging and dual heat treatment. The results show that the two-phase composite microstructure and tri-modal microstructure exhibit better mechanical properties. The above studies show that an equiaxed primary α phase and layered secondary α phase can be obtained after proper heat treatment for TA15 titanium alloys forged by traditional methods, which show excellent comprehensive properties. In addition, the microstructure of the equiaxial α phase and layered α phase can also be obtained by using the heat treatment methods of solution and aging [17,18]. However, there are few reports about the solution and aging treatment of TA15 titanium alloy prepared via SLM. The purpose of our research is to improve the comprehensive mechanical properties of TA15 titanium alloy prepared via SLM at a high temperature by using a solution and aging treatment.

In this study, we analyzed the microstructure of TA15 prepared with SLM and the reason for martensitic grading. Then, we explored the effects of the solution and aging treatment on the microstructure evolution and mechanical properties of TA15. The fracture mechanism was also discussed.

2. Materials and Experimental Procedures

2.1. Materials

SLM has strict requirements for powder. The spherical degree, smooth degree, and size of the powder will affect the overall quality of the final specimens. This study used aerosol TA15 powder provided by AVic Metal Powder Technology Co., Ltd., Beijing, China. The chemical composition of TA15 titanium alloy powder is shown in Table 1. The main chemical elements of TA15 alloy powder are Ti, Al, Zr, Mo, and V. The morphology and particle size distribution of TA15 powder are shown in Figure 1. The spherical diameter is 15–53 μm and 7.76 μm for D10, 16.12 μm for D50, and 27.93 μm for D90.

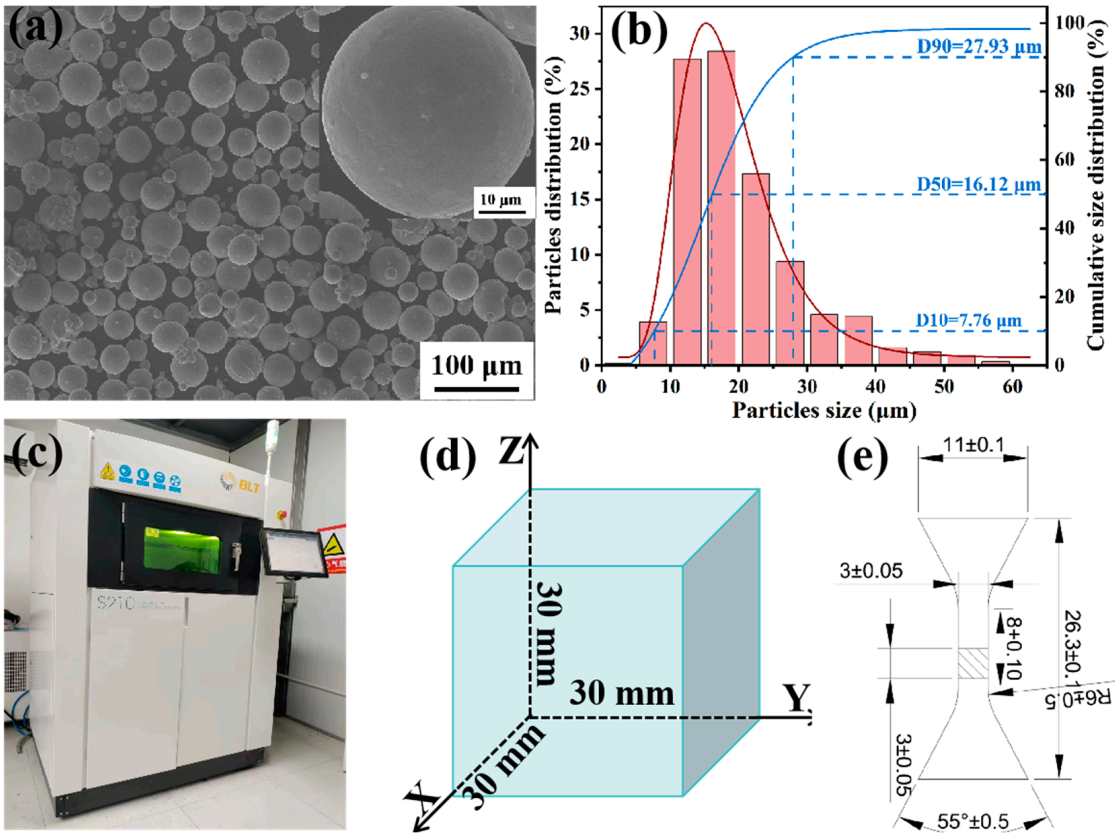


Figure 1. (**a**) Morphology of TA15 titanium alloy power; (**b**) size distribution of TA15 titanium alloy powder; (**c**) SLM machine; (**d**) sample geometry; (**e**) sample geometry for mechanical testing procedures.

Table 1. Chemical composition of TA15 powder.

Element	Ti	Al	V	Zr	Mo	Si	Fe
wt.%	Balance	5.50–7.10	0.80–2.50	1.50–2.50	0.50–2.00	≤0.15	≤0.25

2.2. Sample Fabrications and Heat Treatment Scheme

The selective laser melting (SLM) experiments were conducted by utilizing a BLT-S200 3D printing machine (manufactured by Albot Technology Co., Ltd., Shenzhen, China) with an oxygen concentration maintained at a level below 100 parts per million (ppm). The laser power was set at 180 W, with a scanning rate of 900 mm/s and a scanning interval of 0.06 mm. The TA15 alloy prepared via SLM was heat-treated in a tubular furnace (OTF-1200X, Koji Crystal Material Technology Co., Ltd., Hefei, China), and the heat treatment scheme is shown in Table 2. The heat treatment process involves (i) heating to the preset temperature at a heating rate of 10 °C/min, which is kept for 2 h for water quenching (WQ) to take place; (ii) the temperature is then kept at 600 °C for 4 h, followed by cooling in air (AC).

Table 2. Heat treatment scheme.

No.	Solution Conditions	Aging Conditions
HT1	950 °C/2 h/WQ	600 °C/4 h/AC
HT2	1000 °C/2 h/WQ	600 °C/4 h/AC
HT3	1050 °C/2 h/WQ	600 °C/4 h/AC
HT4	1100 °C/2 h/WQ	600 °C/4 h/AC

2.3. Characterization Method

In this study, an X-ray diffractometer (XRD, Rigaku) was used for phase analysis, a scanning electron microscope (SEM, JSM-IT500HR/LA) for microstructure analysis, and an electron backscatter diffractometer (EBSD, SEM5000) and a transmission electron microscope (TEM, Talos F200s) for analyzing the crystal orientation and crystal structure. The specimens used for microstructure observation were polished using standard metallographic techniques. First, the specimens were polished with 400, 800, 1200, 1600, and 2000 metallographic water-abrasive paper. Then the specimens were polished with a woolen polishing cloth, using diamond spray polishing liquid with a particle size of 1 μm. Finally, a diamond polishing solution with a particle size of 0.5 μm was used for secondary polishing with a velvet polishing cloth. The specimens for EBSD crystal orientation analysis were polished via electrolyzation, and the specimens for TEM crystal structure analysis were thinned using an ion beam.

Tensile experiments were conducted on an electronic universal mechanical machine (American Instron3369) at 600 °C. The geometry of the tensile test is shown in Figure 1e; the fracture was observed via SEM.

3. Results and Discussion

3.1. Influence of Heat Treatment Parameters on Microstructure of TA15 Titanium Alloy

Figure 2 shows the microstructure and XRD pattern of TA15 specimens directly formed via SLM. It can be seen that the microstructure is composed of a large number of differently sized acicular α′ martensite crystals, among which the larger ones are primarily martensite, while the smaller ones are secondary or tertiary martensite. The multiple martensite structure is caused by the local input of high laser energy and the resulting high cooling rate. The α and α + β titanium alloys prepared via SLM usually exhibit a metastable α′ martensite microstructure [19]. In the process of laser melting, when the current powder is melted by using a laser, its heat will also remelt the previous layer of alloy that has already formed a layer, and the structure of the second thermal cycle is then formed. Because of the remelting action, the martensite that has formed a layer will be transformed into a finer second, third, and multistage martensite microstructure [20]. Although the microstructure of multistage martensite contributes to the tensile strength and elongation of the specimen, martensite may undergo phase transition aging under a high-temperature environment, and the failure of the phase transition will lead to a decrease in the mechanical properties, such as the tensile strength of the material.

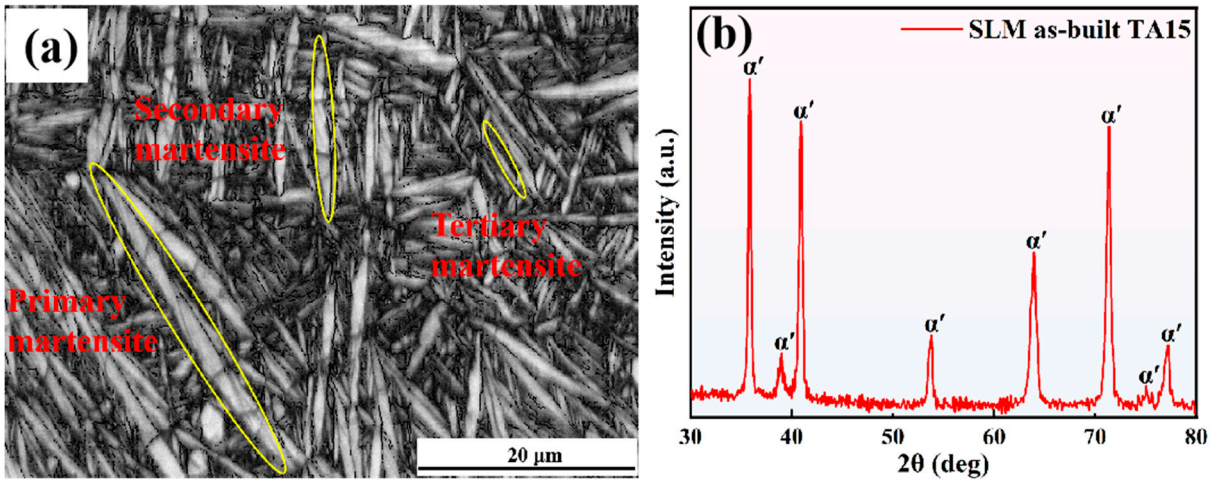


Figure 2. (**a**) Microstructure of SLM as-built TA15; (**b**) XRD patterns of SLM as-built TA15.

Figure 3 shows the microstructure of TA15 titanium alloy specimens formed via SLM after different solution temperatures and aging treatments. With the increase in

the solution temperature, the microstructure of the specimens changed from a typical duplex microstructure (Figure 3a) to an equiaxial microstructure (Figure 3c,f) and then to a Widmanstatten microstructure (Figure 3g), which was decomposed into an equiaxial microstructure after the aging treatment. At the solution temperature of 950 °C, most of the acicular martensite disappeared in the specimen, as shown in Figure 3a. The typical duplex structure with less primary α phase content was formed, in which the white structure was a lamellar mixed structure with alternating secondary α and β phases, and the intermixed black phase was a short rod-like primary α phase, which showed no obvious change after aging treatment. When the solution temperature increased to 1000 °C, the temperature exceeded the β-phase transition temperature. At this temperature, the β-phase microstructure was completely uniform, and the typical equiaxed microstructure was formed (Figure 3c) during water cooling. The primary α phase became larger and equiaxed, and the lamellar secondary α phase precipitated between the primary α phases. After aging treatment, the secondary α phase was further precipitated, and the microstructure became more uniform, as shown in Figure 3d. The average size of the primary α phase was 12.34 μm, and the average thickness of the secondary α phase was 3.9 μm. As the solution temperature further increased to 1050 °C, the size of the primary α phase in Figure 3e increased, and the primary α phase also presented an equiaxial shape.

Additionally, the microstructure became more uniform after aging treatment. The average size of the primary α phase was 25.02 μm, and the average thickness of the secondary α phase was 3.18 μm. At a solution temperature of 1100 °C, the microstructure was completely composed of a β-transition microstructure due to the high temperature, and the secondary α phase was mainly a lamellar and typical Widmanstatten microstructure. After aging treatment, the Widmanstatten microstructure decomposed into a larger primary α phase and an elongated secondary α phase. In this case, the average size of the α phase increased to 39.52 μm, and the average thickness of the secondary α phase decreased to 1.35 μm. It can be seen from the microstructure that the primary α phase appears equiaxed, the size of the primary α phase increases with the increase in the solution temperature, and the thickness of the lamellar secondary α phase decreases. The microstructure changes, and the strength and plasticity of the specimen, may also change accordingly.

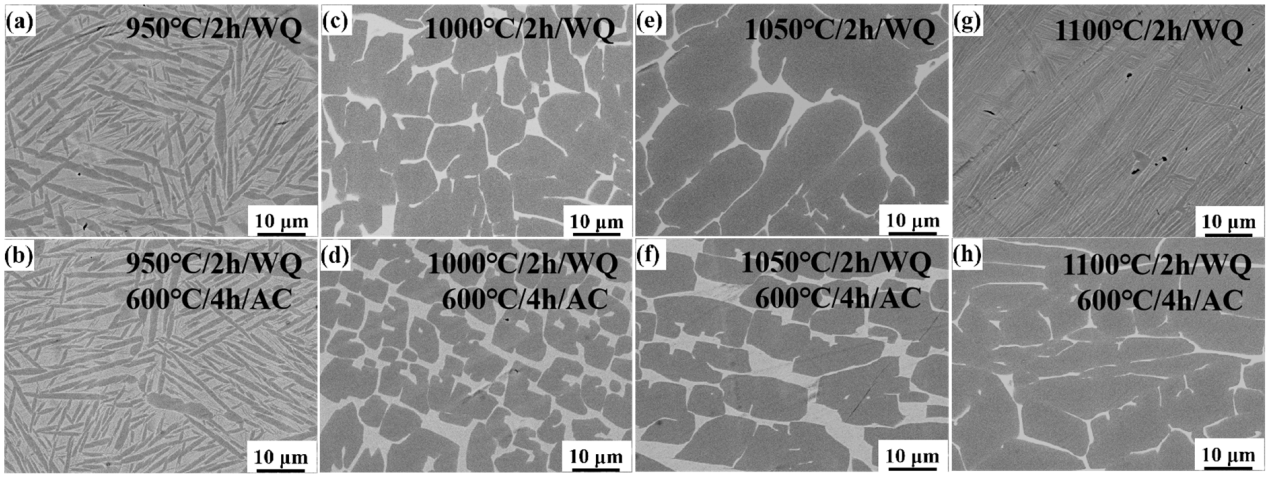


Figure 3. Microstructure after different heat treatments of SEM: (**a**) 950 °C/2 h/WQ; (**b**) 950 °C/2 h/WQ and 600 °C/4 h/AC; (**c**) 1000 °C/2 h/WQ; (**d**) 1000 °C/2 h/WQ and 600 °C/4 h/AC; (**e**) 1050 °C/2 h/WQ; (**f**) 1050 °C/2 h/WQ and 600 °C/4 h/AC; (**g**) 1100 °C/2 h/WQ; (**h**) 1100 °C/2 h/WQ and 600 °C/4 h/AC.

To further discuss the effect of the solution and aging treatment on the specimen's microstructure, the crystal orientation and crystal structure of SLM as-built TA15 and HT2-TA15 were analyzed. The grain orientation, the distribution of orientation misorientation angles, and the pole diagram are shown in Figure 4. The microstructure of TA15 changed significantly before and after the solution and aging treatment, from acicular α´ martensite

(Figure 4a) to equiaxed α phases (Figure 4d), and the secondary α phase precipitated between equiaxed α phases. In addition, it could be seen from the pole diagram (Figure 4c,f) that the texture of TA15 titanium alloys changed significantly before and after the solution and aging treatment, and the texture index increased from 24.81 to 169.73 after the solution and aging treatment. Compared with the SLM as-built TA15, more grains grew in the same crystal direction (01–10) after the solution and aging treatment; the texture degree was higher [21]. In addition, according to the statistics of the misorientation angle in Figure 4b,e, compared with the untreated specimen, the small-angle grain boundary (<10°) of the specimen decreased after the solution and aging treatment, while the large-angle grain boundary (>10°) increased. The large-angle grain boundary mainly makes crack propagation difficult, which is conducive to improving the toughness of the alloy [22].

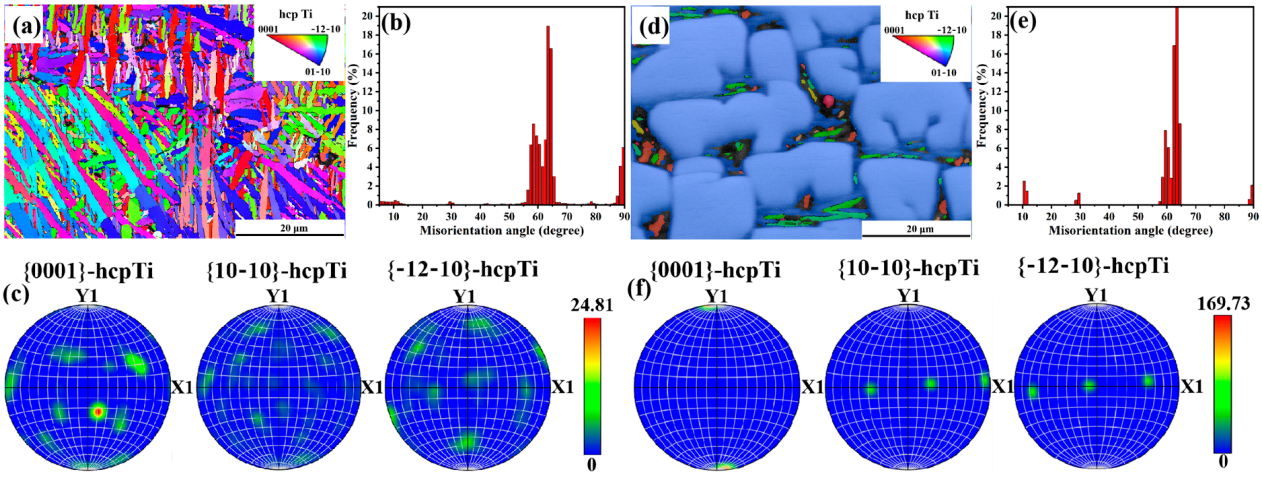


Figure 4. EBSD-derived images of the tested alloys: (**a**,**d**) IPF map of the SLM as-built TA15 and HT2-TA15, respectively; (**b**,**e**) the misorientation angle distribution of the SLM as-built TA15 and HT2-TA15, respectively; (**c**,**f**) the pole diagram of the SLM as-built TA15 and HT2-TA15, respectively.

Figure 5 shows the TEM images of the SLM as-built TA15 and TA15-HT2 alloys. The typical morphology of SLM as-built TA15 is shown in Figure 5a. Figure 5h,i proves that the equiaxed α phase and secondary α phase are Hexagonal Close Packed structures. As a result of heat treatment at higher temperatures, α′ martensite was fully decomposed due to the induction of the non-diffused transformation of α′ martensite, so the α′ martensite hierarchy retained a large number of crystal defects [23]. Figure 5d–f shows that martensite contained many dislocations and coherent twin interfaces. During the solution treatment process, primary, secondary, and tertiary α′ martensite conversions occurred simultaneously, and α′ martensite gradually returned to the α phase. Due to the diffusion of the elements, during the decomposition of martensite, Al elements were concentrated in the HCP phase, while V elements were expelled [24–26], which resulted in α complement nuclei along the original α′ boundary and the formation of β phases at the newly formed α boundary. The heterogeneous nucleation of the β phase occurred mainly at the grain boundaries of martensitic grains. With the gradual precipitation of the secondary α phase in the β phase, the composition of the primary α phase approached a more balanced state. Therefore, during the whole process of heat treatment, the martensite was decomposed into the primary α phase and the secondary α phase [27]. Different temperatures result in different contents and sizes of the primary α phase and secondary α phase, which results in a difference in the performance of the specimen.

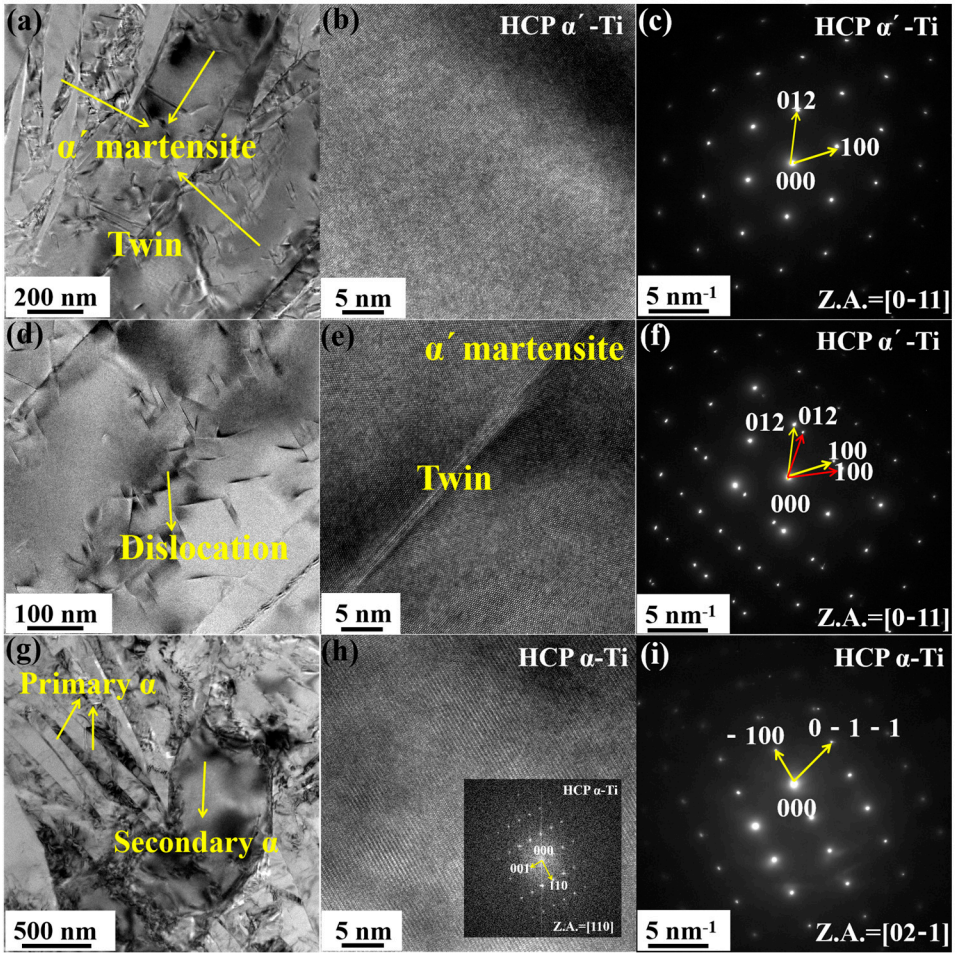


Figure 5. TEM results of SLM as-built TA15: (**a**) bright-field image; (**b**) HRTEM image of martensite; (**c**) SAD patterns of martensite (Z.A. = Zone Axis); (**d**) magnified image of (**a**); (**e**) HRTEM image of nano-size twin; (**f**) SAD patterns of twin. TEM results of HT2-TA15: (**g**) bright-field image; (**h**) HRTEM image of primary α and fast Fourier transformation; (**i**) SAD patterns of secondary α.

3.2. Influence of Heat Treatment Parameters on Mechanical Properties of TA15 Titanium Alloy

A high-temperature tensile test was conducted on SLM as-built TA15 and its heat-treated specimen at 600 °C, and the results of its tensile strength and elongation are shown in Figure 6. With the increase in the heat treatment temperature, the tensile strength of the specimen first increased and then decreased. This is because the size of the equiaxed primary α phase gradually increases with the increase in temperature. In a certain range, more and larger equiaxed α phases are beneficial to the ductility of the specimen. Equiaxed α phases, which are too large, may lead to the formation of holes in the grain or the uneven deformation of the grain, thus reducing the plasticity of the material. It could be seen that when the solution temperature was 1000 °C, the tensile strength at 600 °C was 715 MPa, which was higher than that of other titanium alloys, e.g., 500–625 MPa for TA15 alloy prepared by using Hot Isostatic Pressing at 500–700 °C [28] and about 550 MPa for TiB/TA15 [29].

It could also be seen that the elongation gradually increased and then decreased with the increase in temperature. This is because the width of the layered secondary α phase decreases gradually, and more and thicker-layered secondary α phases in a certain range are conducive to the high-temperature strength of the specimen. Layered α phases can increase the deformation resistance of the material by resisting the movement of dislocation to improve the strength. As the temperature rose to 1050 °C, the elongation peaked at 25.5%, which was higher than that of other titanium alloys, e.g., 10.1–21.9% for TA15 prepared

using annealed Laser Powder Bed Fusion [30]. On the one hand, the equiaxed α phases enhance the plasticity of the specimen; on the other hand, the laminar α phase enhances the strength of the specimen, which endows the specimen with a stable microstructure and good comprehensive mechanical properties [31].

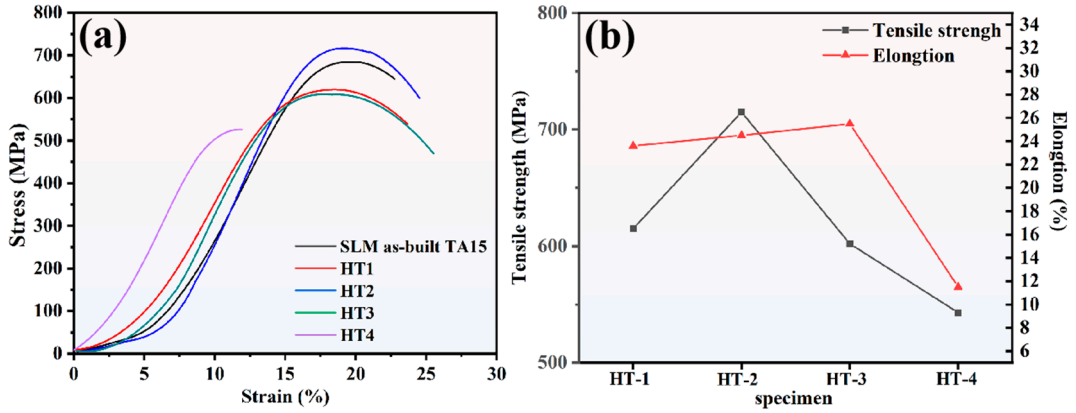


Figure 6. (**a**) Strain stress curve of tensile engineering at 600 °C; (**b**) variation trend of tensile strength and elongation.

To further understand the differences in the tensile behavior of SLM as-built TA15, the tensile fracture behavior was analyzed, and the fracture morphology was observed. Figure 7a shows the fracture morphology of the original specimen. There were small and dense dimples on the fracture surface, showing a ductile fracture mode, which coincided with the good comprehensive mechanical properties of the original specimen. Figure 7b–d shows the fracture morphologies of HT1, HT2, and HT3, respectively, all of which showed obvious dimple characteristics. With the increase in the heat treatment temperature, the dimples grew increasingly larger, corresponding to the gradually increasing elongation in Figure 6b because the larger the dimple size, the higher the elongation. Figure 7e shows the fracture morphology of HT4. Compared with the previous specimens, the fracture presented a very shallow dimple without any obvious cleavage plane trace. Despite the presence of ductile fracture dimples, the appearance of the cleavage plane reduced its plasticity, so HT4 exhibited a mixed fracture morphology and poor ductility. These results are consistent with the significant deterioration of the tensile properties.

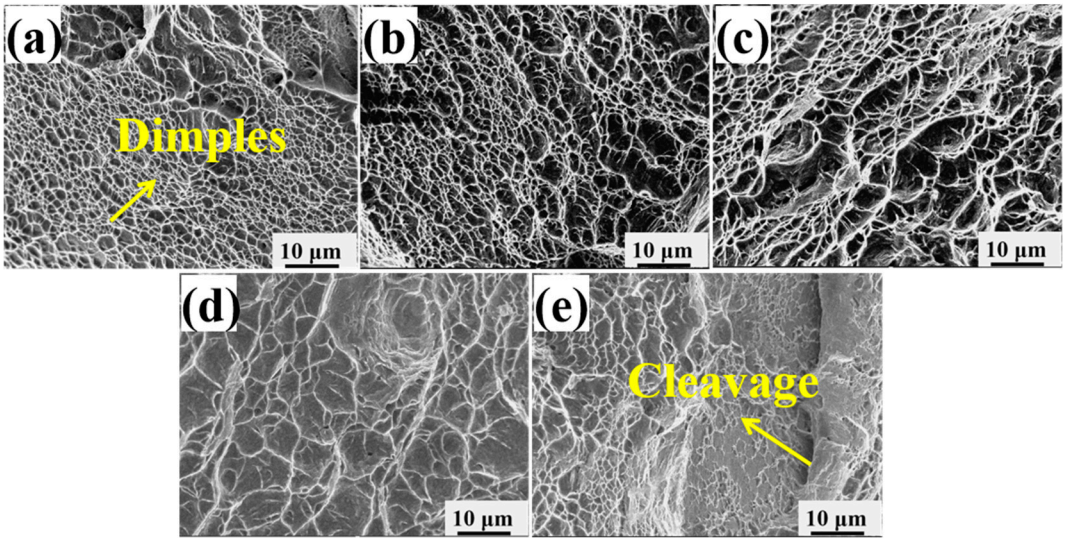


Figure 7. Microscopic fracture morphology of tensile samples: (**a**) SLM as-built TA15; (**b**) HT1; (**c**) HT2; (**d**) HT3; (**e**) HT4.

According to the above results and analysis, it can be inferred that appropriate solution and aging heat treatment can improve the microstructure of SLM as-built TA15 and enhance its comprehensive mechanical properties at a high temperature. The microstructure evolution of SLM as-built TA15 is shown in Figure 8, in which the decomposition of martensite, the growth of equiaxial primary α phases, and the precipitation and growth of secondary α phases are the main factors affecting the comprehensive mechanical properties of the alloy. The first rapidly cooled laser melting process led to a martensite α′ phase formation. In this process, the formed α′ phase contained a high density of lattice defects, such as dislocations and twin crystals. When solid solution heat treatment was performed, residual dislocation was activated, and the Gibbs free energy of the lattice system was reduced through motion, which resulted in the aggregation of dislocation cells and dislocation walls [32]. As the dislocations moved and aggregated, sub-grain boundaries were formed within the α′ phase. Sub-grain boundaries are the interfacial regions of lattice misalignments in different directions in the crystal. Due to dislocation aggregation and the formation of sub-grain boundaries, subsaturated beta stabilizers repelled from the α′ phase. They accumulated at the newly formed sub-grain boundaries, which resulted in the formation of beta phases at such locations. These small α grains were expanded by equiaxed growth. These dislocations also provided pathways for atom migration from the supersaturated solid solution to the secondary α phase core, which gradually grew and aggregated with surrounding atoms to form secondary α grains through atom diffusion. Therefore, the microstructure of the specimens after heat treatment changed from a martensite structure to a typical equiaxed structure, in which equiaxed α phases showed better ductility than other grain structures and the secondary α phase contributed to the good strength of the specimens through microstructure enhancement and hindered grain boundary slip [33,34].

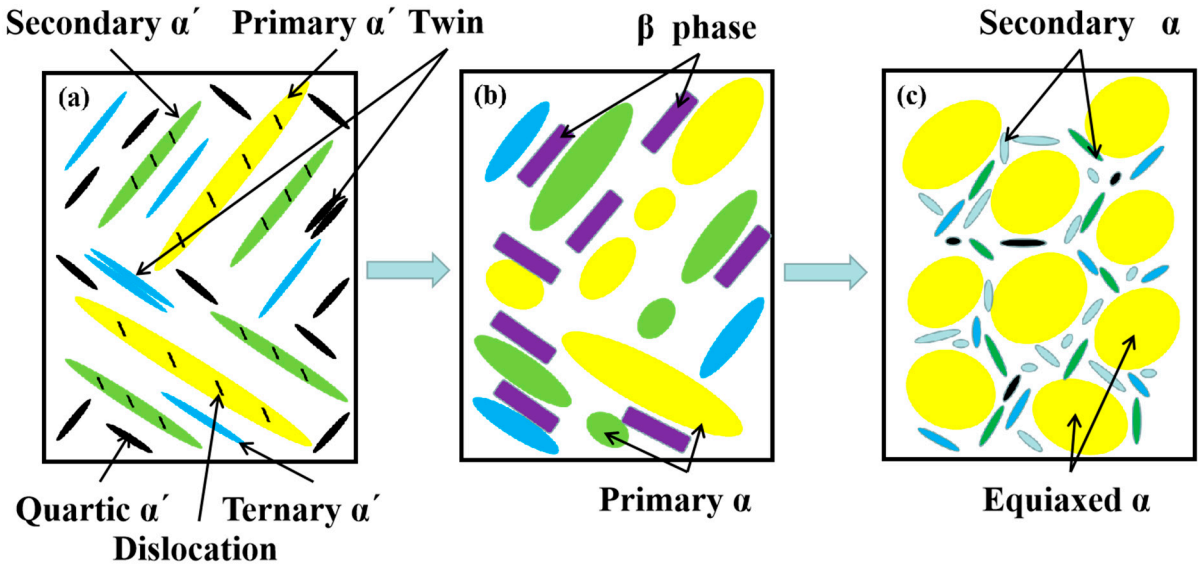


Figure 8. Schematics of microstructures in different tenses: (**a**) SLM as-built TA15; (**b**) in solution; (**c**) after solution and aging.

4. Conclusions

The mechanical properties of TA15 titanium alloys prepared via SLM were further improved by solution and aging treatment. The main conclusions we have drawn are as follows:

1. There are a lot of acicular α′ martensite crystals in the TA15 titanium alloy prepared via SLM, as well as many dislocations and twins in the martensite, which result in good mechanical properties. After solution and aging treatment, martensite is decomposed into equiaxed primary α phases and layered secondary α phases with good mechanical properties.

2. In a certain range, with the increase in the solution temperature, the size of the equiaxed primary α phases gradually increases, and the plasticity of the specimen gradually increases, but the thickness of the layered secondary α phase gradually decreases, accompanied by the gradual reduction in specimen strength. After solution at 1000 °C and aging, the specimens show the best comprehensive mechanical properties, i.e., a high-temperature tensile strength of 715 MPa and corresponding elongation of 24.5%.
3. Firstly, martensite is decomposed into primary and secondary α phases, and the mechanical properties of TA15 titanium alloys are improved through the formation of a phase transition interface and lattice distortion. Secondly, the equiaxed primary α phase and layered secondary α phase improve the mechanical properties and stability of TA15 titanium alloys by hindering the slip and movement of grain boundary dislocations.

Author Contributions: Conceptualization, Q.W. and B.J.; Methodology Q.W. and Y.S.; Software, W.G.; Investigation, X.L. and A.P.; Validation, X.L. and Y.S.; Resources, L.Z.; Data curation, Q.W. and Y.S.; Writing-original draft preparation, Q.W.; Writing-review and editing, Q.W., Y.S. and L.Z.; Supervision, X.D., X.Z. and L.Z. All authors have read and agreed to the published version of the manuscript.

Funding: This research was funded by [Natural Science Foundation of Zhejiang Province] grant number [2021C01023] and the APC was funded by [Natural Science Foundation of Zhejiang Province] grant number [2021].

Data Availability Statement: The data presented in this study are available on request from the corresponding author.

Conflicts of Interest: The authors declare no conflict of interest.

References

1. Liu, Y.; Wu, Z.; Wang, Q.; Zhao, L.; Zhang, X.; Gao, W.; Xu, J.; Song, Y.; Song, X.; Zhang, X. Optimization of Parameters in Laser Powder Bed Fusion TA15 Titanium Alloy Using Taguchi Method. *Crystals* **2022**, *12*, 1385. [CrossRef]
2. Huang, S.; Sun, B.; Guo, S. Microstructure and Property Evaluation of TA15 Titanium Alloy Fabricated by Selective Laser Melting after Heat Treatment. *Opt. Laser Technol.* **2021**, *144*, 107422. [CrossRef]
3. Wang, D.; Li, H.; Zheng, W. Oxidation Behaviors of TA15 Titanium Alloy and TiBw Reinforced TA15 Matrix Composites Prepared by Spark Plasma Sintering. *J. Mater. Sci. Technol.* **2020**, *37*, 46–54. [CrossRef]
4. Zhang, P.; He, A.N.; Liu, F.; Zhang, K.; Jiang, J.; Zhang, D.Z. Evaluation of Low Cycle Fatigue Performance of Selective Laser Melted Titanium Alloy Ti–6Al–4V. *Metals* **2019**, *9*, 1041. [CrossRef]
5. Zhang, S.; Zhang, Y.; Zou, Z.; Shi, Y.; Zang, Y. The Microstructure and Tensile Properties of Additively Manufactured Ti–6Al–2Zr–1Mo–1V with a Trimodal Microstructure Obtained by Multiple Annealing Heat Treatment. *Mater. Sci. Eng. A* **2022**, *831*, 142241. [CrossRef]
6. Tao, P.; Shao, H.; Ji, Z.; Nan, H.; Xu, Q. Numerical Simulation for the Investment Casting Process of a Large-Size Titanium Alloy Thin-Wall Casing. *Prog. Nat. Sci. Mater. Int.* **2018**, *28*, 520–528. [CrossRef]
7. Li, J.; Shen, J.; Hu, S.; Zhang, H.; Bu, X. Microstructure and Mechanical Properties of Ti-22Al-25Nb/TA15 Dissimilar Joint Fabricated by Dual-Beam Laser Welding. *Opt. Laser Technol.* **2019**, *109*, 123–130. [CrossRef]
8. Sun, Q.J.; Xie, X. Microstructure and Mechanical Properties of TA15 Alloy after Thermo-Mechanical Processing. *Mater. Sci. Eng. A* **2018**, *724*, 493–501. [CrossRef]
9. Aksa, H.C.; Hacısalihoğlu, İ.; Yıldız, F.; Varol, T.; Güler, O.; Kaya, G.; Akçay, S.B. Effects of Fabrication Parameters and Post-Processing Treatments on the Mechanical and Tribological Behavior of Surface-Enhanced Copper Based Materials by Selective Laser Melting. *J. Mater. Process. Technol.* **2022**, *304*, 117564. [CrossRef]
10. Varol, T.; Hacısalihoğlu, İ.; Kaya, G.; Güler, O.; Yıldız, F.; Aksa, H.C.; Akçay, S.B. The Effect of Selective Laser Melting Process on the Microstructure, Density, and Electrical Conductivity of Silver-Coated Copper Cores. *J. Mater. Eng. Perform.* **2021**, *30*, 5216–5226. [CrossRef]
11. Wu, X.; Cai, C.; Yang, L.; Liu, W.; Li, W.; Li, M.; Liu, J.; Zhou, K.; Shi, Y. Enhanced Mechanical Properties of Ti-6Al-2Zr-1Mo-1V with Ultrafine Crystallites and Nano-Scale Twins Fabricated by Selective Laser Melting. *Mater. Sci. Eng. A* **2018**, *738*, 10–14. [CrossRef]
12. Cai, C.; Wu, X.; Liu, W.; Zhu, W.; Chen, H.; Qiu, J.C.D.; Sun, C.-N.; Liu, J.; Wei, Q.; Shi, Y. Selective Laser Melting of Near-α Titanium Alloy Ti-6Al-2Zr-1Mo-1V: Parameter Optimization, Heat Treatment and Mechanical Performance. *J. Mater. Sci. Technol.* **2020**, *57*, 51–64. [CrossRef]

13. Jiang, J.; Ren, Z.; Ma, Z.; Zhang, T.; Zhang, P.; Zhang, D.Z.; Mao, Z. Mechanical Properties and Microstructural Evolution of TA15 Ti Alloy Processed by Selective Laser Melting before and after Annealing. *Mater. Sci. Eng. A* **2020**, *772*, 138742. [CrossRef]
14. Li, L.; Pan, X.; Liu, B.; Liu, B.; Li, P.; Liu, Z. Strength and Toughness of Hot-Rolled TA15 Aviation Titanium Alloy after Heat Treatment. *Aerospace* **2023**, *10*, 436. [CrossRef]
15. Sun, Z.C.; Han, F.X.; Wu, H.L.; Yang, H. Tri-Modal Microstructure Evolution of TA15 Ti-Alloy under Conventional Forging Combined with given Subsequent Heat Treatment. *J. Mater. Process. Technol.* **2016**, *229*, 72–81. [CrossRef]
16. Wu, H.; Sun, Z.; Cao, J.; Yin, Z. Formation and Evolution of Tri-Modal Microstructure during Dual Heat Treatment for TA15 Ti-Alloy. *J. Alloys Compd.* **2019**, *786*, 894–905. [CrossRef]
17. Wang, L.; Ma, H.; Fan, Q.; Yao, J.; Shen, X.; Zhang, S.; Zhou, Y.; Peng, Y.; Gao, Y.; Wang, D. Simultaneously Enhancing Strength and Ductility of Ti-6Al-4V Alloy with the Hierarchical Structure via a Novel Thermal Annealing Treatment. *Mater. Charact.* **2021**, *176*, 111112. [CrossRef]
18. Wang, K.; Jiao, Y.; Wu, X.; Qu, B.; Wang, X.; Liu, G. A Novel Composited Process of Solution Treatment-Hot Gas Forming and Stress Relaxation Aging for Titanium Alloys. *J. Mater. Process. Technol.* **2021**, *288*, 116904. [CrossRef]
19. Yang, J.; Yu, H.; Yin, J.; Gao, M.; Wang, Z.; Zeng, X. Formation and Control of Martensite in Ti-6Al-4V Alloy Produced by Selective Laser Melting. *Mater. Des.* **2016**, *108*, 308–318. [CrossRef]
20. Wu, X.; Zhang, D.; Guo, Y.; Zhang, T.; Liu, Z. Microstructure and Mechanical Evolution Behavior of LPBF (Laser Powder Bed Fusion)-Fabricated TA15 Alloy. *J. Alloys Compd.* **2021**, *873*, 159639. [CrossRef]
21. Zhang, Y.; Zhang, S.; Zou, Z.; Shi, Y. Achieving an Ideal Combination of Strength and Plasticity in Additive Manufactured Ti–6.5Al–2Zr–1Mo–1V Alloy through the Development of Tri-Modal Microstructure. *Mater. Sci. Eng. A* **2022**, *840*, 142944. [CrossRef]
22. Wen, P.; Wang, C.; Zhou, P.; Yang, M.; Wang, L.; Wang, B.; Wang, H. Effect of Ultrasonic Treatment on the Microstructure and Mechanical Properties of a New Ni-Base Superalloy 4716MA0. *J. Alloys Compd.* **2022**, *922*, 166278. [CrossRef]
23. Zhao, Z.; Chen, J.; Tan, H.; Zhang, G.; Lin, X.; Huang, W. Achieving Superior Ductility for Laser Solid Formed Extra Low Interstitial Ti-6Al-4V Titanium Alloy through Equiaxial Alpha Microstructure. *Scr. Mater.* **2018**, *146*, 187–191. [CrossRef]
24. Motyka, M.; Baran-Sadleja, A.; Sieniawski, J.; Wierzbinska, M.; Gancarczyk, K. Decomposition of Deformed $\alpha'(\alpha'')$ Martensitic Phase in Ti–6Al–4V Alloy. *Mater. Sci. Technol.* **2019**, *35*, 260–272. [CrossRef]
25. Su, J.; Ji, X.; Liu, J.; Teng, J.; Jiang, F.; Fu, D.; Zhang, H. Revealing the Decomposition Mechanisms of Dislocations and Metastable α' Phase and Their Effects on Mechanical Properties in a Ti-6Al-4V Alloy. *J. Mater. Sci. Technol.* **2022**, *107*, 136–148. [CrossRef]
26. Wu, H.; Sun, Z.; Cao, J.; Yin, Z. Microstructure and Mechanical Behavior of Heat-Treated and Thermomechanically Processed TA15 Ti Alloy Composites. *J. Mater. Eng. Perform.* **2019**, *28*, 788–799. [CrossRef]
27. Cao, S.; Chu, R.; Zhou, X.; Yang, K.; Jia, Q.; Lim, C.V.S.; Huang, A.; Wu, X. Role of Martensite Decomposition in Tensile Properties of Selective Laser Melted Ti-6Al-4V. *J. Alloys Compd.* **2018**, *744*, 357–363. [CrossRef]
28. Cai, C.; Gao, X.; Teng, Q.; Kiran, R.; Liu, J.; Wei, Q.; Shi, Y. Hot Isostatic Pressing of a near α-Ti Alloy: Temperature Optimization, Microstructural Evolution and Mechanical Performance Evaluation. *Mater. Sci. Eng. A* **2021**, *802*, 140426. [CrossRef]
29. Feng, Y.; Zhang, W.; Zeng, L.; Cui, G.; Chen, W. Room-Temperature and High-Temperature Tensile Mechanical Properties of TA15 Titanium Alloy and TiB Whisker-Reinforced TA15 Matrix Composites Fabricated by Vacuum Hot-Pressing Sintering. *Materials* **2017**, *10*, 424. [CrossRef]
30. Liu, J.; Li, Y.; Zhu, Y.; Yang, Y.; Zhang, R.; Zhang, Z.; Huang, A.; Zhang, K. Enhancing High-Temperature Strength and Ductility in Laser Powder Bed Fusion Ti–6.5Al–2Zr–1Mo–1V Alloy via Heat Treatment Optimization. *Mater. Sci. Eng. A* **2022**, *859*, 144201. [CrossRef]
31. Zhang, S.; Zhang, Y.; Qi, J.; Zou, Z.; Qian, Y. Effect of Heat Treatment on the Microstructure and Mechanical Properties of Additive Manufactured Ti-6.5Al-2Zr-1Mo-1V Alloy. *Materials* **2022**, *16*, 160. [CrossRef] [PubMed]
32. Stefansson, N.; Semiatin, S.L. Mechanisms of Globularization of Ti-6Al-4V during Static Heat Treatment. *Metall. Mater. Trans. A* **2003**, *34*, 691–698. [CrossRef]
33. Wang, Q.; Wang, M.; Guo, S.; Tao, S.; Zhou, J.; Qin, Z.; Lin, X.; Huang, W. In Situ Tensile Test of Selective Laser Melted Ti-6.5Al-2Zr-1Mo-1V Alloy at Different Stages of Martensite Decomposition. *J. Mater. Sci.* **2023**, *58*, 1798–1812. [CrossRef]
34. Zhou, Y.; Wang, K.; Li, H.; Wen, X.; Xin, R. Effect of Content and Configuration of Equiaxed α and Lamellar α on Deformation Mechanism and Tensile Properties of a Near-α Titanium Alloy. *Mater. Sci. Eng. A.* **2023**, *877*, 145192. [CrossRef]

Disclaimer/Publisher's Note: The statements, opinions and data contained in all publications are solely those of the individual author(s) and contributor(s) and not of MDPI and/or the editor(s). MDPI and/or the editor(s) disclaim responsibility for any injury to people or property resulting from any ideas, methods, instructions or products referred to in the content.